Experimental Study on Dielectric Constant and Boundary Estimation Method for Double-layered Dielectric Object for UWB Radars

Takuya Niimi, Shouhei Kidera and Tetsuo Kirimoto
Graduate School of Informatics and Engineering,
University of Electro-Communications, Japan
Email: kidera@ee.uec.ac.jp

***Abstract*—A microwave ultra-wideband (UWB) radar system has an advantage for high range resolution and penetrating ability in dielectric object, and is promising for the applications, such as non-destructive testing for aging road or bridge and non-invasive human body inspection. We have already developed an accurate internal imaging approach based on the range points migration (RPM) method, combined with the efficient dielectric constant estimation method. However, the former method is applicable to only the situation that high conductive target is buried into a homogeneous dielectric medium, and is not suitable for the case of multi-layered dielectric structure, such as human body or layered concrete object. As a simple expansion aiming at multi-layered dielectric object, this paper proposes a novel dielectric constant and boundary extraction method for a double-layered case, where the exiting Envelope method is appropriately extended to boundary extraction of the inner layer. The results from finite-difference time-domain (FDTD) based numerical simulation and experiment, demonstrate the effectiveness of our proposed method.**

***Index Terms*—UWB radars, Dielectric constant estimation, Boundary extraction, Non-destructive testing, Range points migration (RPM) method, Inverse scattering**

I. Introduction

There are intensive demands for an innovative imaging techniques aiming at an object embedded in dielectric medium, which is promising for non-invasive medical screening of human body or and monitoring sensor for aging road or bridge. Microwave UWB (Ultra Wideband) radar system becomes one of the most promising technologies with the advantage for higher range resolution and ability to penetrate dielectric objects. In the inverse scattering issue, various reconstruction algorithms for target buried in the dielectric medium have been developed, for example the time-reversal method [1] and the space-time beamforming method [2]. However, these methods are based on the waveform focusing approach assuming point-wise target, and then, the accuracy or spatial resolution is often insufficient for not point-wise target and its computational burden becomes enormous for extension to the 3-D problem.

For a promising approach of the above problem, we have already proposed a high-speed and accurate internal imaging method, based on the extended principle of the RPM method [3]. This study also revealed that the imaging accuracy seriously depends on the assumed dielectric constant, which should be estimated in the practical application. There are various methods for reconstructing both the real and imaginary parts of permittivity, so called inverse scattering analysis, such as the numerical or analytical solution for domain integral equations [4]. However, this type of approaches requires the multidimensional optimization for the discretized space of the region of interest (ROI), and the number of variable dimensions must be severely constrained to avoid sluggish convergence in the optimization process. While other approaches such as in [5] require less computational burden by using the geometric optics (GO) approximation, they assume only a simple and known structure of the dielectric medium, such as a cuboid, and need to accurately estimate a dielectric boundary and its normal vector, beforehand.

For this background, we have already developed a promising method of simultaneously obtaining an accurate internal image and estimating a dielectric constant of surrounding medium [6]. This method employs the range points migration (RPM) [7] and the Envelope interpolation methods [8] to correctly reconstruct dielectric boundary points and their normal vectors at a stage prior to internal imaging. The actual time delay of the propagating through the dielectric medium can then be accurately estimated from the recorded transmissive data. However, this method only assumes the situation that a high conductive object, such as metal, is buried in a single-layered homogeneous medium.

To alleviate this limitation, this paper extends the method [6] to deal with a double-layered dielectric medium at the basic step for multi-layered dielectric object. In this method, the extended Envelope method is introduced to reconstruct the inner boundary points and their normal vectors, and the GO based dielectric constant estimation is adopted to reduce a required computational resources. The results from both numerical and experimental simulations demonstrate that our proposed method simultaneously determines both dielectric constant and each boundary of layered dielectric object, without *a priori* information of shape of each layer.

II. System and observation model

Figure 1 shows the system model. This paper deals with the two-dimensional problem, for simplicity. It is assumed that a dielectric object has a double layer structure. The region for outer and inner medium are defined as $\Omega_{\rm A}$ and $\Omega_{\rm B}$. Two

978-1-4673-6555-0/15/$31.00 ©2015 IEEE

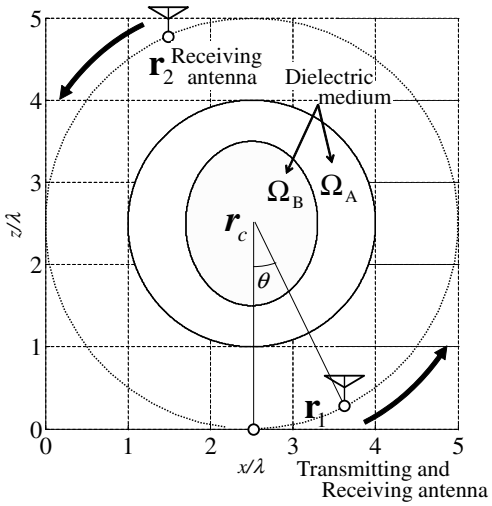

Fig. 1. System and observation model.

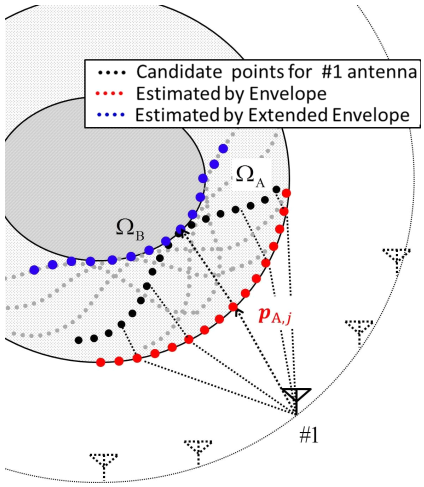

Fig. 2. Principle of extended Envelope method.

omni-directional antennas are scanned along the circle with a center $\boldsymbol{r}_c$ and radius R_c that completely surrounds a dielectric object as shown in Fig. 1. A set of transmitting and receiving antenna is located at $\boldsymbol{r}_1 = (X_1, Z_1)$, and an antenna playing only a receiving role is located at $\boldsymbol{r}_2 = (X_2, Z_2)$, where $\boldsymbol{r}_c = (\boldsymbol{r}_1 + \boldsymbol{r}_2)/2$ is fixed. A center wavelength of transmitting signal is defined as λ. $S_1(X, Z, R)$ and $S_2(X, Z, R)$ are defined as the output of the Wiener filter at antenna positions $\boldsymbol{r}_1$ and $\boldsymbol{r}_2$, respectively, where $R = ct/2$ is expressed by time t and the propagation speed of the radio wave c in the air. The range points extracted from the local maxima of $S_1(X, Z, R)$ and $S_2(X, Z, R)$ are defined as $\boldsymbol{q}_1 = (X_1, Z_1, R_1)$ and $\boldsymbol{q}_2 = (X_2, Z_2, R_2)$, respectively, and this process is detailed in [6]. Each set including $\boldsymbol{q}_1$ and $\boldsymbol{q}_2$ is denoted $\mathcal{Q}_1$ and $\mathcal{Q}_2$, respectively.

III. Conventional Method

We have already proposed the accurate internal imaging method, which accomplishes an accurate dielectric constant and boundary extraction for the situation that a high conductivity target is buried in homogeneous dielectric medium [6]. This method sequentially employs the RPM [7] and the Envelope interpolation methods [8] to correctly reconstruct dielectric boundary points and their normal vectors. The actual time delay of the microwave propagating through the dielectric medium can then be accurately estimated from the recorded transmissive data.

It has been verified that this method accurately estimates the dielectric constant of the medium surrounding an embedded target with considerably lower computational cost than that required by the conventional approaches solving the domain integaral equation [4]. In addition, this method has an advantage over the methods described in [5], which are typically used in the through-the-wall applications, in that it does not require *a priori* knowledge about the shape of the dielectric object. However, this method can only be applied to a limited object model, such as a single-layered homogeneous medium, in principle.

IV. Proposed Method

To alleviate the limitation aforementioned in Sec. III, this paper extends the former method [6] to a double-layered dielectric medium. Here we introduce a new extended Envelope method that reconstructs the inner-layer boundary points and their normal vectors for the propagation path calculation. We also estimate the dielectric constants of both layers by a GO-based method. The methodology is detailed below.

A. Boundary estimation with extended Envelope method

In this method, the set of range points $\boldsymbol{q}_{\mathrm{A},1}$, denoted as $\mathcal{Q}_{\mathrm{A},1}$, is extracted from $\mathcal{Q}_1$, where $S_1(\boldsymbol{q}_{\mathrm{A},1})$ has the maximum value at each antenna location (X, Z). Then, the outer dielectric boundary point is obtained by the Envelope method with the range points $\boldsymbol{q}_{\mathrm{A},1}$ by the method [6] described in Sec. III, and these boundary points and including set are denoted $\boldsymbol{p}_{\mathrm{A},i}$, and $\partial\hat{\Omega}_{\mathrm{A}}$, respectively. Second, the remaining range points are extracted from $\mathcal{Q}_1$ as $\boldsymbol{q}_{\mathrm{B},1}$, where the set of all $\boldsymbol{q}_{\mathrm{B},1}$ denoted as $\mathcal{Q}_{\mathrm{B},1}$ should satisfy $\mathcal{Q}_{\mathrm{B},1} = \mathcal{Q}_1 \cap \overline{\mathcal{Q}_{\mathrm{A},1}}$. Here, to reconstruct an inner dielectric boundary as $\partial\Omega_{\mathrm{B}}$, the existing envelope method [8] is extended as follows. Figure 2 shows the reconstruction principle of the extended Envelope method. In this method, the candidate curve for the inner boundary point of each range point $\boldsymbol{q}_{\mathrm{B},1}$ is calculated using the estimated outer dielectric boundary points $\boldsymbol{p}_{\mathrm{A},i}$ and their normal vector under the Snell's law. using the assumed the dielectric constant of Ω_{A} as ϵ_{A}. The outer envelope of these candidates curve is then extracted as the inner dielectric boundary $\partial\hat{\Omega}_{\mathrm{B}}$. These inner boundary points are denoted $\boldsymbol{p}_{\mathrm{B},j} = (x_{\mathrm{B},j}, z_{\mathrm{B},j})$ $(j = 1, ..., N_{\mathrm{B}})$. N_{B} is the total number of inner boundary estimation points.

B. Dielectric constant estimation by transmissive delay

Next, the methodology for determining each dielectric constant for the region Ω_{A} and Ω_{B} is explained as follows. As

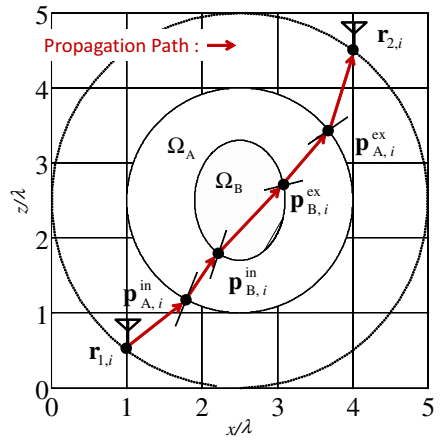

Fig. 3. Propagation path estimation in the proposed method.

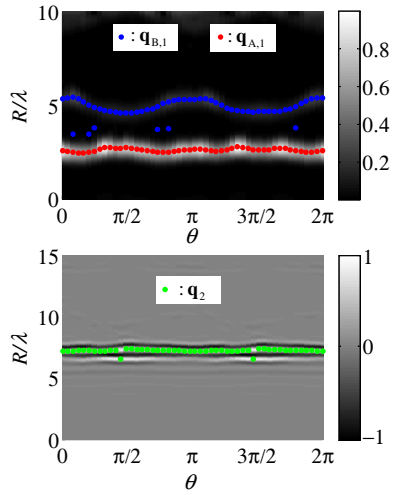

Fig. 4. Wiener filter outputs $S_1(X,Z,R)$ (upper) and $S_2(X,Z,R)$ (lower).

similar to the approach in method [6], this method estimates each dielectric constant by minimizing an observed and calculated transmissive delay. As a first step, the set of incident and exit points of each boundary as $\left(\hat{\boldsymbol{p}}^{\mathrm{in}}_{\mathrm{A},i}, \hat{\boldsymbol{p}}^{\mathrm{in}}_{\mathrm{B},i}, \hat{\boldsymbol{p}}^{\mathrm{ex}}_{\mathrm{B},i}, \hat{\boldsymbol{p}}^{\mathrm{ex}}_{\mathrm{A},i}\right)$ on the dielectric boundary are determined by Snell's law as;

$$\begin{aligned}&\left(\hat{\boldsymbol{p}}^{\mathrm{in}}_{\mathrm{A},i}, \hat{\boldsymbol{p}}^{\mathrm{in}}_{\mathrm{B},i}, \hat{\boldsymbol{p}}^{\mathrm{ex}}_{\mathrm{B},i}, \hat{\boldsymbol{p}}^{\mathrm{ex}}_{\mathrm{A},i}\right)\\ &= \underset{(\boldsymbol{p}_{\mathrm{A},j}, \boldsymbol{p}_{\mathrm{B},k}, \boldsymbol{p}_{\mathrm{B},l}, \boldsymbol{p}_{\mathrm{A},m}) \in \partial\hat{\Omega}_{\mathrm{A}}{}^2 \times \partial\hat{\Omega}_{\mathrm{B}}{}^2}{\arg\min} \Big(\left|\left|\boldsymbol{e}_j(\epsilon_0, \epsilon_{\mathrm{A}}) - \boldsymbol{e}_{j,k}\right|\right|^2\\ &\quad + \left|\left|\boldsymbol{e}_k(\epsilon_{\mathrm{A}}, \epsilon_{\mathrm{B}}) - \boldsymbol{e}_{k,l}\right|\right|^2 + \left|\left|\boldsymbol{e}_l(\epsilon_{\mathrm{B}}, \epsilon_{\mathrm{A}}) - \boldsymbol{e}_{l,m}\right|\right|^2\\ &\quad + \left|\left|\boldsymbol{e}_m(\epsilon_{\mathrm{A}}, \epsilon_0) - \boldsymbol{e}_{m,2}\right|\right|^2 \Big). \end{aligned} \tag{1}$$

Here, $\boldsymbol{e}_j(\epsilon_0, \epsilon_{\mathrm{A}}) = \boldsymbol{R}^{\mathrm{rot}}(\theta_j(\epsilon_0, \epsilon_{\mathrm{A}}))(-\boldsymbol{e}_{\mathrm{n},j})$ holds, where $\boldsymbol{R}^{\mathrm{rot}}(*)$ denotes the 2-D rotation matrix, $\boldsymbol{e}_{\mathrm{n},j}$ is the normal unit vector on target point $\boldsymbol{p}_{\mathrm{A},j}$, and $\theta_j(\epsilon_0, \epsilon_{\mathrm{A}})$ is the refraction angle from the media with ϵ_0 to the media with ϵ_{A} determined by the Snell's law. $\boldsymbol{e}_k(\epsilon_{\mathrm{A}}, \epsilon_{\mathrm{B}})$, $\boldsymbol{e}_l(\epsilon_{\mathrm{B}}, \epsilon_{\mathrm{A}})$ and $\boldsymbol{e}_m(\epsilon_{\mathrm{A}}, \epsilon_0)$ are similarly defined as the above. Also, $\boldsymbol{e}_{1,j}, \boldsymbol{e}_{j,k}, \boldsymbol{e}_{k,l}\boldsymbol{e}_{l,m}$ and $\boldsymbol{e}_{m,2}$ are defined as a unit vector between to two target or antenna location points.

Next, for each range point $\boldsymbol{q}_{2,i}$, the propagation delay from $\boldsymbol{r}_{1,i}$ to $\boldsymbol{r}_{2,i}$ as $\tilde{R}_i(\epsilon_{\mathrm{A}}, \epsilon_{\mathrm{B}})$ is calculated as follow

$$\begin{aligned}\tilde{R}_i(\epsilon_{\mathrm{A}}, \epsilon_{\mathrm{B}}) &= \left|\left|\hat{\boldsymbol{p}}^{\mathrm{in}}_{\mathrm{A},i} - \boldsymbol{r}_{1,i}\right|\right| + \sqrt{\epsilon_{\mathrm{A}}}\left|\left|\hat{\boldsymbol{p}}^{\mathrm{ex}}_{\mathrm{A},i} - \hat{\boldsymbol{p}}^{\mathrm{in}}_{\mathrm{B},i}\right|\right|\\ &+ \sqrt{\epsilon_{\mathrm{B}}}\left|\left|\hat{\boldsymbol{p}}^{\mathrm{in}}_{\mathrm{B},i} - \hat{\boldsymbol{p}}^{\mathrm{ex}}_{\mathrm{B},i}\right|\right| + \sqrt{\epsilon_{\mathrm{A}}}\left|\left|\hat{\boldsymbol{p}}^{\mathrm{ex}}_{\mathrm{B},i} - \hat{\boldsymbol{p}}^{\mathrm{ex}}_{\mathrm{A},i}\right|\right|\\ &+ \left|\left|\hat{\boldsymbol{p}}^{\mathrm{ex}}_{\mathrm{A},i} - \boldsymbol{r}_{2,i}\right|\right|. \end{aligned} \tag{2}$$

Figure 3 also shows an example of propagation path and the incident and exit points of each boundary. The dielectric constants for dielectric media for $\boldsymbol{q}_{2,i}$ are determined as;

$$(\hat{\epsilon}_{\mathrm{A},i}, \hat{\epsilon}_{\mathrm{B},i}) = \underset{(\epsilon_{\mathrm{A}}, \epsilon_{\mathrm{B}})}{\arg\min} \left| R_{2,i} - \tilde{R}_i(\epsilon_{\mathrm{A}}, \epsilon_{\mathrm{B}}) \right|^2. \tag{3}$$

Finally, using all the transmissive range points $\boldsymbol{q}_2$, the optimal dielectric constants are determined as

$$(\hat{\epsilon}_{\mathrm{A}}, \hat{\epsilon}_{\mathrm{B}}) = \frac{\sum_{i=1}^{N_2} S_2(\boldsymbol{q}_{2,i})(\hat{\epsilon}_{\mathrm{A},i}, \hat{\epsilon}_{\mathrm{B},i})}{\sum_{i=1}^{N_2} S_2(\boldsymbol{q}_{2,i})}, \tag{4}$$

where N_2 is the total number of range points $\boldsymbol{q}_2$.

V. Performance Evaluation

A. Evaluation in Numerical Simulation

As described in Sec. II, the two antennas located as $\boldsymbol{r}_1$ and $\boldsymbol{r}_2$ are simultaneously scanned on the circumference of circle radius 2.5λ and center is $\boldsymbol{r}_{\mathrm{c}} = (2.5\lambda, 2.5\lambda)$, where the data are observed 50 points with an equal interval for the range as $0 \le \theta \le 2\pi$. Each received signal on $\boldsymbol{r}_1$ and $\boldsymbol{r}_2$ is generated by FDTD, assuming TE mode wave. Assuming typical parameters of concrete, the dielectric constants of the outer and inner dielectric media are set to $\epsilon_{\mathrm{A}} = 3.0$ and $\epsilon_{\mathrm{B}} = 6.0$, respectively, and the conductivity of each medium is set to 0.01 S/m. A noiseless situation is assumed. The upper and lower sides of Fig. 4 show the outputs of the Wiener filter as $S_1(X,Z,R)$ and $S_2(X,Z,R)$. As shown in the upper panel of Fig. 4, the range points reflected from the outer and inner boundaries ($\boldsymbol{q}_{\mathrm{A},1}$ and $\boldsymbol{q}_{\mathrm{B},1}$, respectively) are clearly separated. However, there are some unnecessary range points in $\boldsymbol{q}_{\mathrm{B},1}$ that precede the desired range points. These undesirable signals are caused by a side-lobe echo effect from the boundary of $\partial\Omega_{\mathrm{A}}$, because they appear when $\boldsymbol{q}_{\mathrm{A},1}$ and $\boldsymbol{q}_{\mathrm{B},1}$ approach each other. The dielectric constants estimated from Eq. (4) are $\hat{\epsilon}_{\mathrm{A}} = 3.21$ (relative error of 10%) and $\hat{\epsilon}_{\mathrm{B}} = 6.62$ (relative error of 11%). Figure 5 shows the dielectric boundary reconstructed by the Envelope and extended Envelope methods, using the estimated dielectric constants of both media. The lower panel enlarges the region enclosed by the blue boundary in the upper panel. This figure reveals that, although the envelope method accurately expresses the outer boundary $\partial\Omega_{\mathrm{A}}$, the extended version does not precisely estimate the inner boundary $\partial\Omega_{\mathrm{B}}$. This can

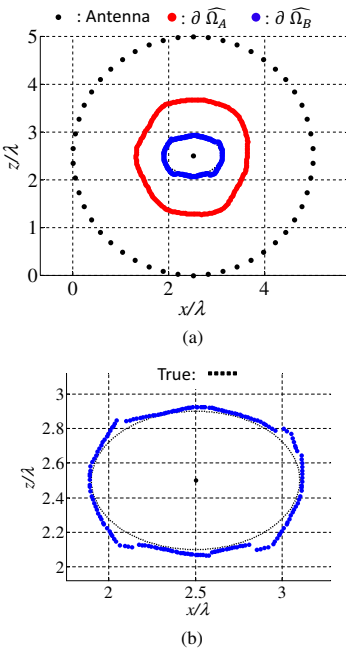

Fig. 5. (a) Estimated dielectric boundaries for $\Omega_{\rm A}$ and $\Omega_{\rm B}$ using the proposed method, (b): Enlarged view for $\Omega_{\rm B}$.

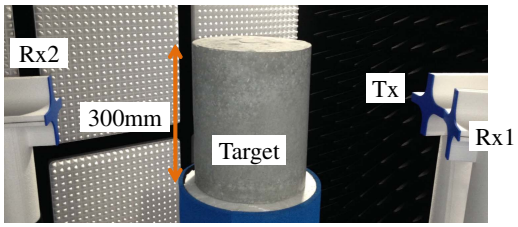

Fig. 6. Experimental setup.

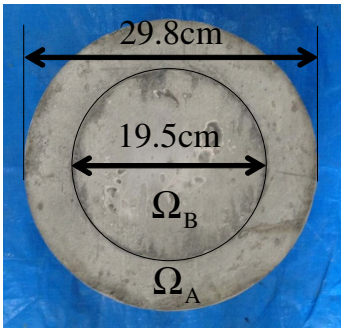

Fig. 7. Concrete target with double-layered structure.

be explained by that an antenna $\boldsymbol{r}_1$ cannot receive a strong echo from the inner boundary area, which is not accurately reconstructed, due to the path skewed by the concave part of outer boundary. In addition, the root-mean-square errors (RMSEs) of outer and inner boundary are $1.1 \times 10^{-2}\lambda$ and $3.4 \times 10^{-2}\lambda$, respectively.

B. Evaluation with Experimental Data

In this subsection, the proposed method is evaluated in an experiment configured in an anechoic chamber. The experimental setup is illustrated in Fig. 6. The antenna is a cross-dipole antenna in vertical polarization mode. The single transmitting antenna is located at $\boldsymbol{r}_{\rm T}$, and the signal data $S_1(X, Z, R)$ and $S_2(X, Z, R)$ are observed at the two receiving antennas $\boldsymbol{r}_{\rm R1}$ and $\boldsymbol{r}_{\rm R2}$, respectively. To accomplish the circular scanning model described in Sec. II, the dielectric object is rotated about the center $\boldsymbol{r}_{\rm C}$, fixing the location of the antennas $\boldsymbol{r}_{\rm T}$, $\boldsymbol{r}_{\rm R1}$ and $\boldsymbol{r}_{\rm R2}$. To guarantee a sufficient accuracy for target manufacturing at the order of 1/100 transmitting wavelength (around 1 mm), this experiment assumes a simple shape case. Specifically, a cylindrical mortal mix $\Omega_{\rm B}$ is buried in the cylindrical cement $\Omega_{\rm A}$, and both cylinders are 300mm high. The radii of the mortal and cement mediums are 298 mm and 195 mm, respectively. The actual dielectric constants of the dielectric object (cement and mortal) are measured as 10.95 and 9.70 by assessing the propagation delay in the case that a known simple dielectric object with each material is used. The target rotation center is set to $\boldsymbol{r}_{\rm C} = (400{\rm mm}, 400{\rm mm})$, and the distance from the antenna, namely, $R_{\rm C}$ is set to 400 mm. The received signal is obtained using a VNA (Vector Network Analyzer), where the frequency is swept from 1000 MHz to 3000 MHz at 10 MHz intervals. S_1, S_2 are obtained by applying the inverse discrete Fourier transform to the acquired frequency data. The effective bandwidth is around 2.0 GHz, corresponding to a range resolution of approximately 75 mm. The center frequency is also 2.0 GHz (center wavelength : 150 mm).

Here, the average S/Ns of $S_1(X, Z, R)$ and $S_2(X, Z, R)$ are 42 dB, 34 dB, respectively, where the S/N is defined as the ratio of the peak instantaneous signal power to average noise power after applying a matched filter. In addition, to suppress the range sidelobe caused by relatively narrower fractional bandwidth of the transmitted signal compared with that assumed in numerical simulation, the Capon filter is used for range point extraction, which is detailed in [9]. The upper and lower sides of Fig. 8 show the outputs of the Capon filter as $S_1^{\rm CP}(X, Z, R)$ and $S_2^{\rm CP}(X, Z, R)$ in the experimental case, respectively. Note the undesirable signals around $R = 0.9$ m in the $S_2^{\rm CP}(X, Z, R)$ output. These are attributed to a creeping wave propagating along the dielectric outer boundary. We previously developed a method that suppresses creeping signals without *a priori* knowledge of the outer dielectric boundary [10]. Applying this method to $S_2^{\rm CP}(X, Z, R)$, we obtained the actual transmissive delays (plotted as the range points $\boldsymbol{q}_2$ in the bottom panel of Fig. 8).

In this case, the estimated dielectric constants using Eq. (4) in the proposed method, are $\hat{\epsilon}_{\rm A} = 10.68$ (relative error of 2.5%) and $\hat{\epsilon}_{\rm B} = 9.02$ (relative error of 7%), respectively. Figure 9 shows each reconstructed image of the double layered dielectric media, as $\partial\hat{\Omega}_{\rm A}$ and $\partial\hat{\Omega}_{\rm B}$, respectively, where the estimated dielectric constants are used for the extended Envelope method. Note that, since the bi-static radar model is used in this experiment, the both boundary estimated methods,

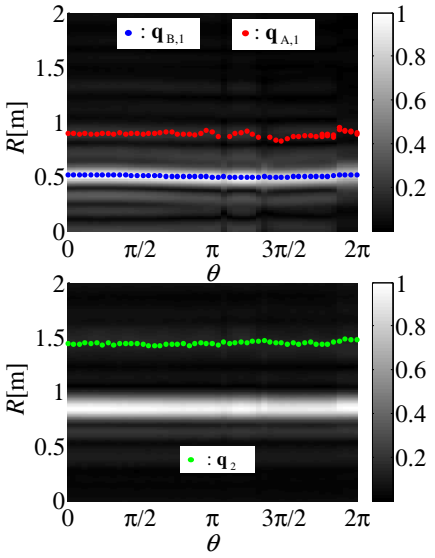

Fig. 8. Output of Capon method of two-layer object.

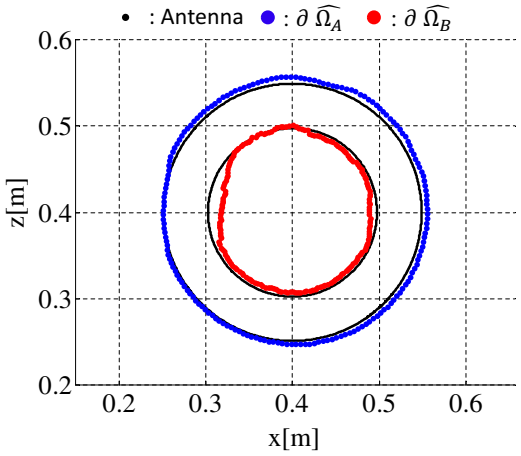

Fig. 9. Estimated dielectric boundaries for Ω_{A} and Ω_{B} using the proposed method in the experiment.

as the Envelope and the extended Envelope methods, are modified to this observation model. The RMSEs of outer and inner boundary are about 6.5 mm ($4.3 \times 10^{-2}\lambda$) and 7.7 mm ($5.1 \times 10^{-2}\lambda$), respectively. This result confirms that our proposed method enables highly accurate boundary extraction in realistic scenarios; indeed, the accuracy is on the order of 1/100 of the transmitting wavelength, which is sufficient for practical applications. However, as shown in Fig. 9, part of the estimated inner boundary $\partial\Omega_{\mathrm{B}}$ is rendered inaccurate by errors in the range points, which are introduced by side-lobe effects or clutters. Because the accuracy and resolution of the range point extraction directly affects the accuracy of the dielectric constant and boundary estimates, the accuracy or resolution of the range points should be improved by adopting super-resolution techniques.

VI. Conclusion

This paper proposed an accurate estimation method for dielectric constants and boundary shapes of double-layered dielectric object. As a notable feature of this method, it is applicable to arbitrary target shape, and offers an accurate estimation for both dielectric constant and boundary extraction without *a priori* knowledge of shape of each boundary. In addition, this method exploits a unique characteristic of newly developed Envelope method extended to inner boundary extraction, which accurately offers not only boundary points but also normal vector on them. This feature enables us to determine the possible propagation path penetrating into double-layered dielectric medium using Snell's law. The results obtained from both numerical simulation and experimental investigation revealed that our proposed method provided a considerably accurate dielectric constant estimation, which contributes each boundary extraction with the accuracy at the order of 1/100 transmitting center wavelength.

Acknowledgment

This work was supported by Grant-in-Aid for Young Scientists (A) by JSPS KAKENHI Grant Number 26709030, and the Yazaki Memorial Foundation.

References

[1] P. Kosmas, and C. M. Rappaport, "A Matched-Filter FDTD-Based Time Reversal Approach for Microwave Breast Cancer Detection," *IEEE Trans. Antennas Propagat.*, vol. 54, no. 4, pp. 1257–1264, Apr., 2006.

[2] X. Li, E. J. Bond, B. D. Van Veen, and S. C. Hagness, "An overview of Ultra-Wideband Microwave Imaging via Space-Time Beamforming for Early-Stage Breast-Cancer Detection," *IEEE Antennas Propagat. Mag.*, vol. 47, no. 2, pp. 19–34, Feb., 2005.

[3] K. Akune, S. Kidera, and T. Kirimoto, "Accurate and Nonparametric Imaging Algorithm for Targets Buried in Dielectric Medium for UWB Radars," *IEICE Trans. Electronics*.vol. E95-C, no. 8, pp. 1389–1398, Aug., 2012.

[4] R. Autieri, M. Urso, T. Isernia, and V. Pascazio, "Inverse Profiling via an Effective Linearized Scattering Model and MRF Regularization," *IEEE Trans. Geosci. & Remote Sens.*, vol. 8, no. 6, pp. 1021–1025, Nov., 2011.

[5] J. Ren, Y. Zhang, T. Jiang, and W. Chen, "Estimation of Wall Parameters From Time-Delay-Only Through-Wall Radar Measurements," *IEEE Trans. Antennas Propagat.*, vol. 59, no. 11, pp. 4268–4278, Nov., 2011.

[6] R. Souma, S. Kidera and T. Kirimoto, "Accurate Permittivity Estimation Method with Iterative Waveform Correction for UWB Internal Imaging Radar" *IEICE Trans. Electronics*. vol. E96, no. 5, pp. 730-737, May., 2013.

[7] S. Kidera, T. Sakamoto, and T. Sato, "Accurate UWB Radar 3-D Imaging Algorithm for Complex Boundary without Range Points Connections," *IEEE Trans. Geosci. Remote Sens.*, vol. 48, no. 48, pp. 1993-2004, Apr., 2010.

[8] S. Kidera, T. Sakamoto, and T. Sato," A Robust and Fast Imaging Algorithm with an Envelope of Circles for UWB Pulse Radars," *IEICE Trans. Commun.*, vol. E90-B, no. 7, pp. 1801–1809, Apr., 2007.

[9] S. Kidera, T. Sakamoto and T. Sato, "Super-Resolution UWB Radar Imaging Algorithm Based on Extended Capon with Reference Signal Optimization," *IEEE Trans. Antennas. & Propagation.*, vol.59, no. 5, pp. 1606–1615, May, 2011.

[10] T. Manaka, S. Kidera and T. Kirimoto, "Experimental Study on Permittivity Estimation Method for UWB Internal Imaging Radar", 2014 International Symposium on Antennas and Propagation (ISAP2014), Dec., 2014.